Sixth International Symposium on Turbulence and Shear Flow Phenomena
Seoul, Korea, 22-24 June 2009

LARGE SCALE STRUCTURE OF TURBULENT BOUNDARY LAYER SUBJECTED TO AN ADVERSE PRESSURE GRADIENT

Joung-Ho Lee
Corporate Research & Development Division
Hyundai-Kia Motors
772-1 Jangduk-Dong, Hwaseong-Si, Gyeonggi-Do, 445-706, Korea
jholee@hyundai.com

Hyung Jin Sung
Department of Mechanical Engineering,
KAIST
373-1 Guseong-dong, Yuseong-gu, Daejeon, 305-701, Korea
hjsung@kaist.ac.kr

ABSTRACT

The effects of adverse pressure gradients on turbulent structures were investigated by carrying out direct numerical simulations of turbulent boundary layers subjected to adverse pressure gradients. The equilibrium adverse pressure gradient flows were established by using a power law free-stream distribution $U_\infty \sim x^m$.. Estimates of the conditionally averaged velocity fields associated with the spanwise vortical motion were obtained by using linear stochastic estimation. These results confirm that the outer region of the adverse pressure gradient boundary layer is populated with streamwise-aligned vortex organizations.

INTRODUCTION

Turbulent boundary layers (TBLs) are subjected to adverse pressure gradients (APGs) in numerous engineering applications, such as diffusers, turbine blades and the trailing edges of airfoils. The upper limit of the efficiency of such devices is almost always determined by the APG, so the behaviour of APG flow is of practical importance. Understanding the coherent structures in TBLs is essential to understanding boundary layer turbulence. Since organized motions play a crucial role in the production of wall turbulence, the study of coherent structures contributes to the accuracy of turbulence models and advances in flow control strategies (Robinson, 1991). Therefore elucidating the behaviour of the coherent structures in APG TBLs provides insight into the physics of APG flow and improves its modelling.

Many important features of APG TBLs are quite well understood. In general, as the magnitude of an APG increases, the mean velocity profile develops a large wake region and the turbulent kinetic energy decreases in the near-wall region (Nagano et al. 1993). In an experimental study of an APG TBL, Skåre & Krogstad (1994) found that the statistics in the outer layer are significantly affected by a strong APG. However, little is known about the effect of APG on coherent structures in TBLs. The main objective of this study was to examine statistically the effects of APGs on the coherent structures of TBLs.

In the present study, we simulated a spatially developing turbulent boundary layer with adverse pressure gradient using direct numerical simulation in order to elucidate the effect on the outer layer turbulent structures of adverse pressure gradient. First the numerical method is described briefly and some results are compared with the flows with zero pressure gradient.

NUMERICAL METHODS

Direct numerical simulations are performed to investigate the physics of spatially developing turbulent boundary layer flows subjected to adverse pressure gradient. A schematic diagram of the computational domain is displayed in Fig. 1. Time-dependent zero pressure gradient turbulent inflow data are provided at the inlet based on the method of Lund *et al.* (1998). A convective boundary condition at the exit has the form $(\partial u/\partial t) + c(\partial u/\partial x) = 0$, where c is the local bulk velocity. The no-slip condition is imposed at the solid wall. Periodic boundary conditions are applied in the spanwise direction. Townsend (1961) and Mellor & Gibson (1966) showed that an approximate equilibrium flow is obtained when the variation of free-stream has the form of a power-law relation in the streamwise direction. A free-stream velocity $U_\infty(x)$ along the upper boundary of the computational domain is prescribed as,

$$U_\infty(x) = U_0\left(1 - \frac{x}{x_0}\right)^m \qquad (1)$$

where m denotes the exponent of adverse pressure gradient (Fig. 2). Four cases are considered, defined by the exponent of adverse pressure gradient summarized in Table 1.

Our method simulates without any assumptions on the evolution of boundary layer and no extra terms are added to the Navier-Stokes equations. The Navier-Stokes equations are integrated in time using the fractional step method with an implicit velocity decoupling procedure proposed by Kim *et al.* (2002). All the terms are discretized with Crank-Nicolson method in time, the coupled velocity components in the convection term are decoupled by the implicit

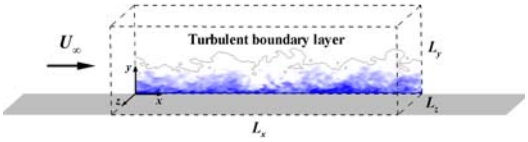

Fig. 1: Schematic diagram of computational domain.

Table 1: Case parameters

Designation	m	x_0	Re_θ
ZPG	0	∞	1410
APG1	-0.150	-200	770 ~ 1035
APG2	-0.200	-200	1125 ~ 1290

velocity decoupling procedure. The decoupled velocity components are solved without iteration. Since the implicit decoupling procedure relieves the CFL restriction, the computation time is significantly reduced. The mesh is uniform in the streamwise and spanwise directions. However a hyperbolic tangent distribution is used in the wall-normal direction. The mesh resolutions are $\Delta x^+ = 12.5$, $\Delta y^+_{min} = 0.17$, $\Delta y^+_{MAX} = 24$ and $\Delta z^+ = 5$ based on the friction velocity at the inlet. The computational time step used is $\Delta t^+ = 0.25$.

RESTULTS AND DISCUSSION

Various results indicating the presence of low-momentum regions (LMRs) and packets of hairpin vortices in ZPG flows have recently been reported (Adrian *et al*., 2000; Ganapathisubramani *et al*., 2003). Although several types of structures are present in the outer layers of TBLs, it appears that elongated LMRs and hairpin packets are the dominant outer layer structures associated with turbulence production (Ganapathisubramani *et al*. 2003). LMRs and coherent groups of vortices are also present throughout the outer layers of APG flows. Fig. 2 shows a visualization of an instantaneous flow field subjected to a strong APG. Several elongated low-speed regions are present in the outer layer and each of them lies beneath a group of streamwise-aligned hairpin-like structures.

Galilean decomposition has been used to detect swirling motions in flows. If the convection velocity is subtracted from the flow field, velocity vectors with a streamwise component that is similar to the selected convection velocity have a small magnitude, so such regions appear light in the visualization. Vortex patterns moving with a velocity equal to the subtracted convection velocity are seen in such light regions. Fig. 3 shows the instantaneous velocity fields in the streamwise-wall-normal plane of the boundary layer for the ZPG and APG flows. The velocity fields were processed with the Galilean frames. The swirling strength contours are also shown in the background to highlight the locations of the vortex cores. A single vortex packet is evident in both flows. In the APG flow, several vortex cores are aligned with an inclination angle of about 18° relative to the wall and advect with a similar convection velocity. These vortex cores are associated with the heads of hairpin-like vortices, i.e., cane-like, horseshoe or hairpin vortices. The ejection of

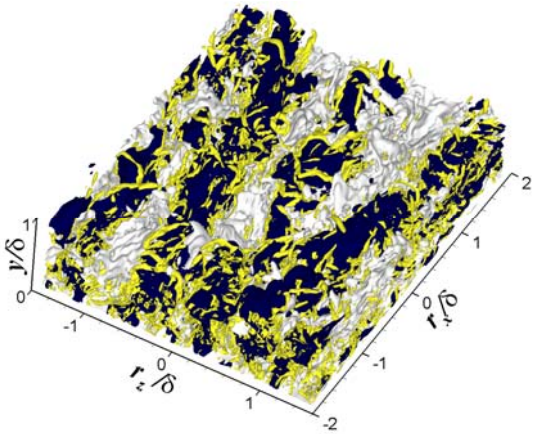

Fig. 2: Outer vortical structures in an adverse pressure gradient boundary layer (β = 1.68). The vortices are shown as yellow iso-surface plots of swirling strength (11% of maximum λ_{ci}). The black and white areas are low- and high-speed regions (10% below and above local free-stream velocity) respectively.

low-speed fluid away from the wall under the vortex is consistent with the hairpin vortex signature introduced by Adrian *et al*. (2000). The inclination angle of the packet in the APG flow is larger than that for the ZPG flow, for which the angle is approximately 13°. However, these large-scale structures are similar to those proposed in the conceptual model of hairpin packets in ZPG TBLs of Adrian *et al*. (2000). These instantaneous fields indicate that vortex packets are common features in the outer regions of TBLs subjected to an APG.

In this section, we discuss these large-scale structures in the outer layers of APG TBLs and their statistical properties.

Stochastic estimation of vortex organization in the outer layer

The above visualizations of instantaneous structures and velocity fields show that hairpin-like vortex organizations are associated with low-momentum regions (LMRs) and are commonly visible in the outer regions of APG TBLs. In this section, we provide statistical evidence that the outer layers of APG TBLs are populated by organizations of vortices aligned coherently in the streamwise direction. To investigate the vortex organizations statistically, we now consider the LSE of the average flow field associated with a single spanwise vortical motion (represented by λ_{ci}). The analysis in this section follows that of Christensen & Adrian (2001). However, their approach to planar PIV data is extended for volumetric DNS data to educe the three-dimensional form of the vortex organization. Here λ_{ci} is calculated from the two-dimensional velocity gradient tensor, $D^{2\text{-}D}$, in the *x*-*y* plane, in order to detect only spanwise swirling motion at a given location if possible. $D^{2\text{-}D}$ can be expressed as,

$$D^{2\text{-}D} = \begin{bmatrix} \partial u/\partial x & \partial u/\partial y \\ \partial v/\partial x & \partial v/\partial y \end{bmatrix} \quad (2)$$

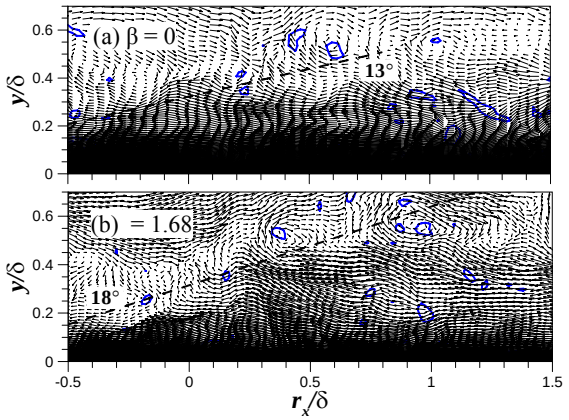

Fig. 3: Instantaneous velocity vector fields with the constant convection velocity removed: (a) β = 0; (b) β = 1.68. Contours of λ_{ci} are shown in the background to highlight the location of the vortex cores.

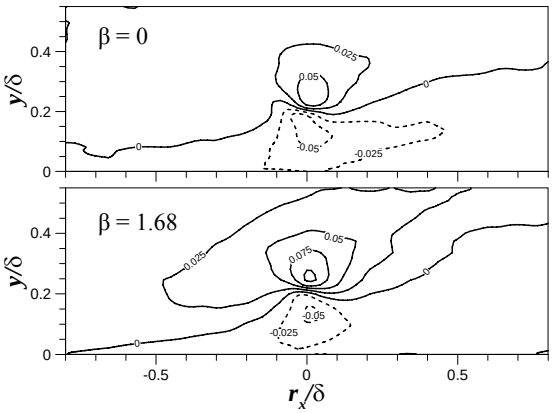

Fig. 4: Two-point correlations between the streamwise velocity and the swirling strength for y/δ = 0.2. Contour levels are from -0.05 to 0.1 with increments of 0.025.

The conditional event is chosen to be a positive λci. The LSE $\hat{u}_i(x+r)$ of this conditional average $\langle u_i(x+r)|\lambda_{ci}(x)\rangle$ is given by (Christensen & Adrian 2001),

$$\hat{u}_i(x+r) = L_i\lambda_{ci}(x)\,, \qquad (3)$$

with i=1, 2, and 3 and

$$L_i = \frac{\langle \lambda_{ci}(x)u_i(x+r)\rangle}{\langle \lambda_{ci}(x)^2\rangle}. \qquad (4)$$

It can be seen from equation (4) that two-point correlations between the swirling strength and the velocity are necessary to calculate the coefficient L_i.

Two-point correlations between swirling strength and velocity. Fig. 4 shows the contours of the two-point correlations between swirling strength and streamwise velocity $R_{\lambda u}$ at y/δ = 0.2. Fig. 5 shows the wall-normal correlation functions $R_{\lambda v}$ for the same location. The present streamwise and wall-normal correlation functions for the ZPG flow are qualitatively consistent with those of Christensen & Adrian (2001), which were obtained from channel data. The contours of correlation show the average velocity field associated with a vortex core located at the reference point. Since the swirling strength always has a positive or zero value, $R_{\lambda u}$ and $R_{\lambda v}$ have the same sign as the streamwise and wall-normal velocities respectively. Thus, the statistically dominant direction of rotation around the vortex core can be determined from the two-point correlations between swirling strength and velocity. In the x-y plane, $R_{\lambda u}$ is positive above the vortex core and negative below the vortex core. $R_{\lambda v}$ is positive left of $r_x^+ = 0$ and negative right of $r_x^+ = 0$ for both the APG and ZPG flows, i.e., the rotation in the spanwise vortices is clockwise. This result implies that spanwise vortices with clockwise rotation are detected in this region more often than those with counterclockwise rotation, which is consistent with the instantaneous visualizations.

When a strong adverse pressure gradient is applied, the spatial extents of the negative $R_{\lambda v}$ regions behind the vortex cores increase. Note that the negative $R_{\lambda v}$ region expands toward the near-wall region for a strong APG flow, as can be seen in Fig. 5 (b). This result indicates that the outer turbulence is transported further toward the wall for a strong APG flow and that this strong downward diffusion is associated with the spanwise vortex in the log layer; it also complements the experimental study of Skåre & Krogstad (1994), which shows that the direction of the turbulent diffusion is reversed, resulting in considerable turbulent transport towards the wall in the TBL near separation. Fig. 5 (c) and (d) show the contours of $R_{\lambda v}$ for ZPG and APG flows in the x-z plane at y/δ = 0.2 respectively. The spanwise extent of negative $R_{\lambda v}$ contours for the APG flow is greater than that for the ZPG flow. The streamwise extent of the positive $R_{\lambda u}$ region is greater for the APG flow than for the ZPG flow. However, the streamwise extent of the negative $R_{\lambda u}$ region is reduced by the downward diffusion mentioned above. For streamwise correlation functions, the inclination angle of the 0-contours is an estimate of the average inclination angle of the outer vortex organization. The inclination angle of the APG flow is larger than that of the ZPG flow.

Vortex organizations educed by linear stochastic estimation. The stochastic estimation of the conditionally averaged velocity fields around the single spanwise vortex at y/δ = 0.2 was performed using the correlation functions described in the previous section. The flow structures educed from the linear estimates are illustrated in Fig. 6. The velocity vectors in the estimated flow fields were set to unit magnitude in order to show the weak motions away from the event location more clearly (Christensen & Adrian 2001). The vortices were visualized using iso-surfaces of λ_{ci} equal to 7% and 10% of its maximum for the ZPG and APG flows respectively. The dark area represents low-speed fluid. The resulting flow structures in the three-dimensional perspective are packets of hairpin-like vortices for both the ZPG (β = 0) and APG (β = 1.68) flows, as shown in Fig. 6 (a) and (b) respectively. It is clear that the spanwise oriented vortex structure is located at the event location, which corresponds to the head of the hairpin-type vortex. This hairpin-like vortex consists of two

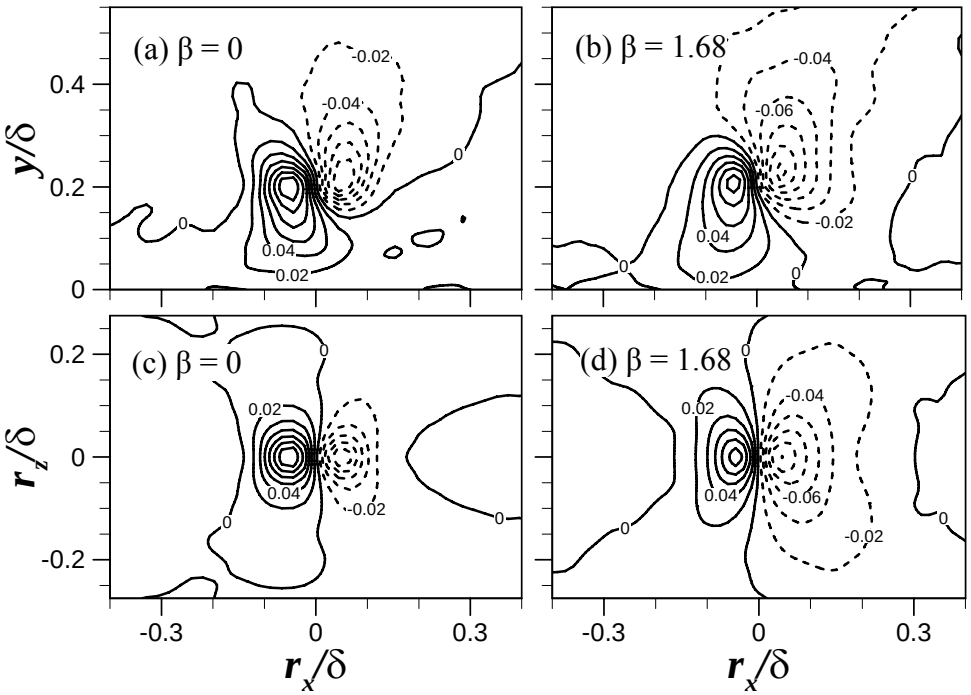

Fig. 5: Two-point correlations between the wall-normal velocity and the swirling strength centered at $y/\delta = 0.2$. x-y plane at $r_z = 0$: (a) $\beta = 0$; (b) $\beta = 1.68$. x-z plane at $y/\delta = 0.2$: (c) $\beta = 0$; (d) $\beta = 1.68$. Contour levels are from -0.12 to 0.12 with

quasi-streamwise legs and a steeply inclined hairpin part. This result suggests that the dominant spanwise swirling motions in the log layer are associated with the hairpin head. The symmetry of the eddies is a consequence of the statistical symmetry of the given event with respect to the reflection about the vertical plane at $r_z^+ = 0$. Of course, many individual structures have asymmetric shapes, as shown in Fig. 2.

Spanwise vortex structures are visible not only at the event location but also both upstream and downstream of this location. This result implies that the vortices are arranged in the streamwise direction with considerable coherence. There is a qualitative similarity between the averaged vortex organization (Fig. 6) and the instantaneous realizations (Fig. 2). Five and four distinct hairpin-like vortices form packets in the ZPG and APG flows respectively and are aligned in the streamwise direction. It is interesting to note that the hairpin legs survive the averaging process even though the streamwise alignment of the hairpin in each packet is not perfect and the spanwise size of the packets varies from packet to packet. A little noise is present in the iso-surface of λ_{ci} away from the event point since the packets in the instantaneous fields are not perfectly aligned in the streamwise direction and the ensembles are not fully converged. However, the ensembles can be used to identify the spanwise vortex structures. There is an elongated low-momentum region beneath the streamwise hairpin packet that is bounded by hairpin vortices. These patterns are consistent with the hairpin vortex packet model of Adrian *et al.* (2000). For $\beta = 0$, compact spanwise vortex structures can be seen, as shown in Fig. 6 (c) (marked A and C). Zhou *et al*. (1999) observed similar spanwise vortices located between quasi-streamwise vortices, and showed that compact spanwise vortices assist the uplift of quasi-streamwise vortices and that the spanwise vortex is then connected with the lifted streamwise vortices. For $\beta = 1.68$, the spanwise extents of the hairpin vortices located at $y/\delta > 0.2$ are relatively insensitive to the distance from the wall. The spanwise extent is about 0.4δ, as shown in Fig. 6 (d).

The velocity vector fields on the x-y plane at $r_z = 0$ for the ZPG and APG flows are shown in Fig. 7 (a) and (b) respectively. The locations of the vortex cores are indicated by the swirling strength contours. It is clear that upward motion of low-speed fluid (Q2) is observed just upstream of and below the vortex core at the event location for both flows. For $\beta = 1.68$, a downward motion of high-speed fluid (Q4) that is stronger than that for $\beta = 0$ appears just behind the vortex core. Spanwise swirling motions are visible not only at the specified event location but also both upstream and downstream of this location. For $\beta = 0$, the vortical motions are inclined away from the wall at an angle of 13°. This result is consistent with the observations of Zhou *et al*. (1999) and Christensen & Adrian (2001). For β=1.68, the inclination angle is approx. 18.5°, which is larger than that for $\beta = 0$. These inclination angles are consistent with the instantaneous realizations in Fig. 3.

For $\beta = 0$, the streamwise separation of the vortex cores varies with the distance from the wall. The streamwise distance between the vortex cores (A) and (B) is approximately 150 viscous wall units (0.23δ). This separation is similar to the experimentally observed

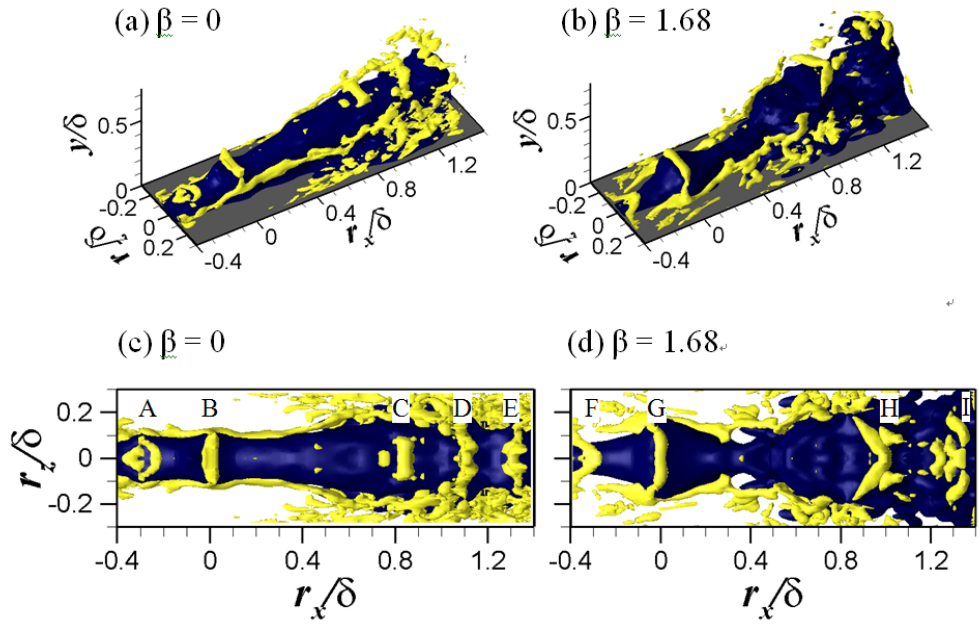

Fig. 6: Vortex organization of the linearly estimated velocity field for a spanwise swirl at $y/\delta = 0.2$. Perspective view: (a) $\beta = 0$; (b) $\beta = 1.68$. Top view: (c) $\beta = 0$; (d) $\beta = 1.68$. The vortices are identified from the yellow iso-surface plots of λ_{ci}.

streamwise separation between hairpin heads within a packet of 100–200 viscous wall units (Adrian *et al.* 2000). Away from the wall, the vortex cores (B) and (C) are separated by approx. 550 viscous wall units (0.83δ). Adrian *et al.* (2000) reported that the vortex spacing is governed by inner scales but increases as the hairpins grow. In contrast, Christensen & Adrian (2001) showed that the average vortex spacing can be scaled with the outer length scale δ regardless of the Reynolds number, with a spacing of approx. 0.3–0.4δ. The spacing is approximately half of the vortex spacing between (B) and (C). The vortex spacing is in good agreement with the results of Christensen & Adrian (2001), except for the region between (B) and (C); they noted that the swirling motion 0.4δ downstream from the event location is not clear. The increased spacing between vortex cores found in the present data might be the result of a vortex that is missing due to the variation of the vortex spacing from packet to packet during the averaging process, as suggested in Christensen & Adrian (2001). However, the swirling patterns of the downstream vortices (C), (D), and (E) are clear. The streamwise spacings between (C) and (D) and between (D) and (E) are approx. 0.28δ and 0.2δ respectively, which are similar to the distance between (A) and (B). These streamwise separations are also similar to the streamwise dimensions of the individual outer conditional eddies. These results suggest that vortices (A) and (C) are secondary vortices generated upstream of the primary vortices (B) and (D) respectively, as reported in Zhou *et al*. (1996), and that the hairpin spacing is governed by both inner and outer variables. The streamwise spacing between the primary and secondary vortices is governed by small scales associated with the streamwise dimensions of individual hairpins, whereas the distance between the primary vortices (B) and (D) is governed by large scales associated with the streamwise dimensions of packets.

The qualitative similarity of the vortex spacing in the APG and ZPG flows is clear. However, the vortex spacing increases when the length scale is normalized by δ, as shown in Fig. 7 (b). The streamwise vortex spacing in a packet is related to the frequency of strong Q2 events. Multiple Q2 events can occur within a single burst event (Bogard & Tiederman 1986). A single burst event is associated with the passage of a hairpin head in a packet (Adrian *et al*. 2000). If the spacing of vortex heads increases (decreases), the frequency of the Q2 events associated with hairpin-like vortices decreases (increases). Krogstad & Skåre (1995) reported that the frequency of Q2 events scaled with outer scaling is reduced and that Q4 events last much longer in the APG flow than in the ZPG flow, in particular for strong events in APG TBLs. This reduction in the frequency of Q2 events can be explained in terms of increases in the streamwise spacing of hairpins in the conditionally averaged packets of the APG flow. The longer durations of Q4 events in the APG flow is related to the increased streamwise extent of the negative $R_{\lambda u}$ region just behind the vortex head.

SUMMARY AND CONCLUSION

The effects of adverse pressure gradients on the structures of turbulent boundary layers have been investigated. A comparison of the structures of ZPG and APG TBLs has been presented. Present results provide the first three-dimensional statistical evidence for packets of hairpin-type vortices in turbulent boundary layers and are based on linear stochastic estimation of the conditionally averaged flow field associated with a single transverse vortex core. The outer region of the turbulent boundary layer is populated with streamwise packets of vortices. Although it may be not possible to detect all hairpins on a

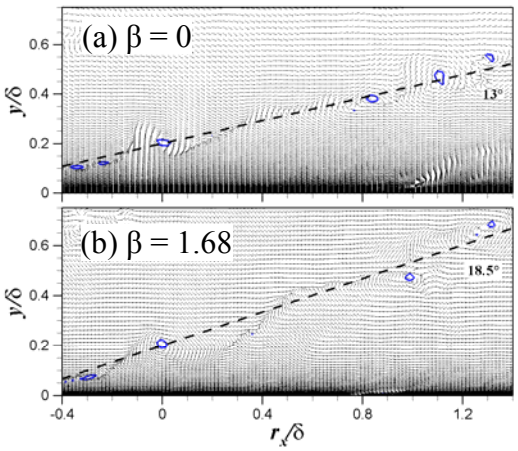

Fig. 7: Linear estimate of the conditional velocity field based on a spanwise swirl at y/δ = 0.2. The locations of the vortex cores are indicated by the swirling strength contours.

packet through the current analysis, the packet of vortices is sufficiently significant in the outer region of the APG to leave a footprint on the results of the conditional average. The vortices are relatively well aligned in the streamwise direction and propagate coherently behind each other. The adverse pressure gradient augments the angle of inclination of the packets and the spacing of the vortex heads. The increase in the streamwise vortex spacing explains the reduction in the frequency of second-quadrant events. We believe that the typical characteristics of a hairpin packet are present in an average sense since multiple hairpin heads and legs in a packet survive the conditional averaging, despite variations in the hairpin arrangement in the instantaneous vortex packets. Studies of much higher Reynolds numbers are needed to determine the overall behavior of hairpin packets since the packets at low Reynolds numbers contain just 3~ 5 vortices.

ACKNOWLEDGEMENTS

The authors would like to acknowledge the support from the Korea Institute of Science and Technology Information under the Grand Challenge Supercomputing Program.

REFERENCES

Adrian, R. J., Meinhart, C. D. & Tomkins, C. D., 2000, "Vortex organization in the outer region of the turbulent boundary layer", *J. Fluid Mech.*,Vol. 422, pp. 1-54.

Christensen, K. T. & Adrian, R. J., 2001, "Statistical evidence of hairpin vortex packets in wall turbulence", *J. Fluid Mech*., Vol. 431, pp. 433-443.

Ganapathisubramani, B., Longmire, E. K. & Marusic, I. 2003, "Characteristics of vortex packets in turbulent boundary layers", *J. Fluid Mech.*, Vol. 478, pp. 35-46.

Kim, K., Baek, S.-J. and Sung, H. J., 2002, "An implicit velocity decoupling procedure for the incompressible Navier-Stokes equations", *Int. J. Numer. Meth. Fluids*, Vol. 38, pp. 125-138.

Krogstad, P. & Skåre, P. E. 1995, "Influence of a strong adverse pressure gradient on the turbulent structure in a boundary layer", *Phys. Fluids*, Vol. 7, pp. 2014-2024.

Lund, T. S., Wu, X. and Squires, K. D., 1998, "Generation of turbulent inflow data for spatially-developing boundary layer simulations", *J. Comput. Phys.*, Vol. 140, pp.233-258.

Mellor, G. L. and Gibson, D. M., 1966, "Equilibrium turbulent boundary layers", *J. Fluid Mech.*, Vol. 24, pp.225-253.

Nagano, Y., Tagawa, M. & Tsuji, T. 1993, Effects of adverse pressure gradients on mean flows and turbulence statistics in a boundary layer. In Turbulent Shear Flows 8, (ed. Durst, F., Friedrich, R., Launder, B.E., Schmidt, F.W., Schumann, U. & Whitelaw, J.H.), pp. 7-21, Springer, Berlin.

Robinson, S. K., 1991, "Coherent motions in the turbulent boundary layer", *Ann. Rev. Fluid Mech.*, Vol.23, pp. 601-639.

Skåre, P. E. and Krogstad, P.-Å, 1994, "A turbulent equilibrium boundary layer near separation", *J. Fluid Mech.*, Vol. 272, pp.319-348.

Townsend, A. A., 1961, "Equilibrium layers and wall turbulence", *J. Fluid Mech.*, Vol. 11, pp. 97-120.

Zhou, J., Adrian, R. J., Balachandar, S. & Kendall, T. M. 1999, "Mechanisms for generating coherent packets of hairpin vortices in channel flow", *J. Fluid Mech.*, Vol. 387, pp. 353-396.